Available online at www.sciencedirect.com
SCIENCE DIRECT
Journal of Power Sources 158 (2006) 225–244
JOURNAL OF POWER SOURCES
www.elsevier.com/locate/jpowsour

Design and partial load exergy analysis of hybrid SOFC–GT power plant

F. Calise [a,*], A. Palombo [a], L. Vanoli [b]

[a] *DETEC, Università degli Studi di Napoli Federico II, P.le Tecchio80, 80125 Naples, Italy*
[b] *Dipartimento di Scienza degli Alimenti, Università degli Studi di Napoli Federico II, Via Università 100, Portici, NA 80055, Italy*

Received 3 June 2005; received in revised form 28 July 2005; accepted 31 July 2005
Available online 19 October 2005

Abstract

This paper presents a full and partial load exergy analysis of a hybrid SOFC–GT power plant. The plant basically consists of: an air compressor, a fuel compressor, several heat exchangers, a radial gas turbine, mixers, a catalytic burner, an internal reforming tubular solid oxide fuel cell stack, bypass valves, an electrical generator and an inverter. The model is accurately described. Special attention is paid at the calculation of SOFC overpotentials. Maps are introduced, and properly scaled, in order to evaluate the partial load performance of turbomachineries. The plant is simulated at full-load and part-load operation, showing energy and exergy flows trough all its components and thermodynamic properties at each key-point. At full-load operation a maximum value of 65.4% of electrical efficiency is achieved. Three different part-load strategies are introduced. The off-design operation is achieved handling the following parameters: air mass flow rate, fuel mass flow rate, combustor bypass, gas turbine bypass, avoiding the use of a variable speed control system. Results showed that the most efficient part-load strategy corresponded to a constant value of the fuel to air ratio. On the other hand, a lower value of net electrical power (34% of nominal load) could be achieved reducing fuel flow rate, at constant air flow rate. This strategy produces an electrical efficiency drop that becomes 45%.

Keywords: SOFC; Exergy; Modeling

1. Introduction

High temperature solid oxide fuel cells (SOFC) are promised to be the most efficient device for direct conversion of fuel chemical energy into electricity. Its efficiency can be further increased when coupled with a gas turbine (GT) cycle up to 70% [1]. The perspective of full commercialization of hybrid SOFC–GT plants is very attractive since these devices could represent the most efficient equipment for residential/distributed power/heat generation applications [1–4]. Theoretically, the lower size of a hybrid SOFC–GT power plant is conditioned only by the smallest commercial available microturbine [1]. According to the present technological progress in microturbine research field, it is possible to assume that hybrid plants could be commercialized from the size of 100 kW up to 10 MW, perfectly suitable for cogeneration distributed plants [1,2].

Nowadays, at least four different types of SOFC are available (tubular, tubular "high power density", planar, and microtubolar) [1,2]. Although these have been studied since 1970s only a few prototypes are presently operating. Siemens Westinghouse is probably the main company involved in the design and commercialization of hybrid SOFC–GT power plants [1–4]. This company installed a 220 kW hybrid tubular SOFC–GT system at the National Fuel Cell Research Center in California. Results coming from these experimental tests showed values of the net electrical efficiency lower than the target ones (52% versus 57%) [1]. This experimental campaign demonstrated the huge difficulty in integrating SOFC with traditional components [1].

Usually, SOFC–GT hybrid plants are designed only at full-load operation [5–8], taking into account the connection with the electrical network, determining an energetic and economic dependence of the plant on the network. This circumstance can be avoided since SOFC–GT hybrid plants are perfectly suitable also as stand alone devices. In fact, as shown in many previous papers [9–11], conversely from the traditional energy conversion devices, these hybrid plants show very slight efficiency

* Corresponding author. Tel.: +39 081 7682304; fax: +39 081 2390364.
E-mail address: frcalise@unina.it (F. Calise).

0378-7753/$ – see front matter © 2005 Elsevier B.V. All rights reserved.
doi:10.1016/j.jpowsour.2005.07.088

Nomenclature

A	heat transfer area (m^2)
c_p	heat specific capacity ($kJ\,kg^{-1}\,K^{-1}$)
C	concentration
D	diffusion coefficient
ex_{ch}	specific chemical exergy ($kJ\,kmol^{-1}$)
E	open circuit reversible potential (V)
E_{act}	activation energy ($kJ\,kmol^{-1}$)
F	Faraday constant ($As\,mol^{-1}$)
G	Gibbs free energy ($kJ\,kmol^{-1}$)
i	current density ($mA\,cm^{-2}$)
i_l	limiting current density ($mA\,cm^{-2}$)
i_0	exchange current density ($mA\,cm^{-2}$)
K	equilibrium constant of reaction
$\dot{m}$	mass flow rate ($kg\,s^{-1}$)
M	molar mass ($g\,mol^{-1}$)
$\dot{n}$	molar flow rate ($kmol\,s^{-1}$)
n_e	number of e^- per mol of H_2 reacted
N	rotor speed (rpm)
p	partial pressure (bar)
P	electrical power (kW)
r	area specific resistance ($\Omega\,cm^2$)
r_{SC}	steam to carbon ratio
R	gas constant ($J\,mol^{-1}\,K^{-1}$)
t	temperature (°C)
T	temperature (K)
U	heat transfer coefficient ($kW\,m^{-2}\,K^{-1}$)
U_f	fuel utilization factor
V	cell potential (V)
V_{act}	activation overpotential (V)
V_{conc}	concentration overpotential (V)
V_{ohm}	ohmic overpotential (V)
x	CH_4 reacted moles ($kmol\,s^{-1}$)
x_i	component molar fraction
y	CO reacted moles ($kmol\,s^{-1}$)
z	H_2 reacted moles ($kmol\,s^{-1}$)

Greek symbols

α	charge transfer coefficient
β	pressure ratio
γ	i_0 equation constant ($mA\,cm^{-2}$)
δ	component thickness (cm)
ε	heat transfer efficiency
η	efficiency
ν_i	stoichiometric coefficient
ρ	resistivity ($\Omega\,cm$)

Subscripts

a	environment
c	correct
cold	cold fluid
DP	design point
el	electrical
ex	exergetic
f	formation
hot	hot fluid
is	isentropic
ref	reference
s	solid

Superscript

°	standard pressure

degradations at partial load, due to the modularity of the cell. Obviously, this goal can be achieved only in case of an optimized design of the plant, both at design and partial load operation, is performed. Consequently, during the last years, some authors [9–11] started investigating the behavior of hybrid plants taking into account the partial load operating conditions. In spite of this effort, research is very far from obtaining satisfactory results, since many technical problems still have to be solved [1,11].

In the present paper, a properly developed plant layout is discussed. A detailed model of all components of the plant is introduced, paying special attention at the electrochemical and chemical reaction occurring within the SOFC. On the basis of this model, different partial load strategies are presented, investigating plant performances and analyzing inefficiencies through plant components, both at full and partial load operation.

2. Plant layout

The selected plant layout (Fig. 1) allows the best compromise between cost, simplicity, reliability and efficiency. During the last period of time, a number of papers have been published introducing dozens of different plant layouts, coupling the SOFC with a number of traditional devices (GT, steam turbine, heat exchangers, gasifiers, biogas recovers, etc.) [1–4]. Usually, the more complex the plant layout is, the higher is its efficiency and, consequently, its capital cost. The choice of plant layout is dramatically affected by the SOFC arrangement [1–11]. In this work it is assumed to use an anode re-circulation arrangement (Fig. 2), that allows to avoid the use of an expensive heat recovery steam generator [9,10]. In this case, in fact, the steam required to support the steam reforming reaction is derived from the anode outlet stream. Obviously, during the start-up, the plant requires an external boiler that produced steam for the reforming reaction. In this paper the start-up is not taken into account, thus the external boiler is not considered. The plant layout under investigation in the present work is displayed in Fig. 1. It consists of: a centrifugal air compressor (AC); a centrifugal fuel compressor (FC); a counterflow tube in tube air–GT exhaust heat exchanger (HE1); a counterflow tube in tube fuel–GT exhaust heat exchanger (HE2); a radial gas turbine (GT); mixers for anode re-circulation (M) and air bypass (M_{GT}); a catalytic burner (CB); an internal reforming tubular solid oxide fuel cell stack (IRSOFC); a counterflow air-SOFC exhaust heat exchanger (HE_{SOFC}); bypass valves; an electrical generator and an inverter.

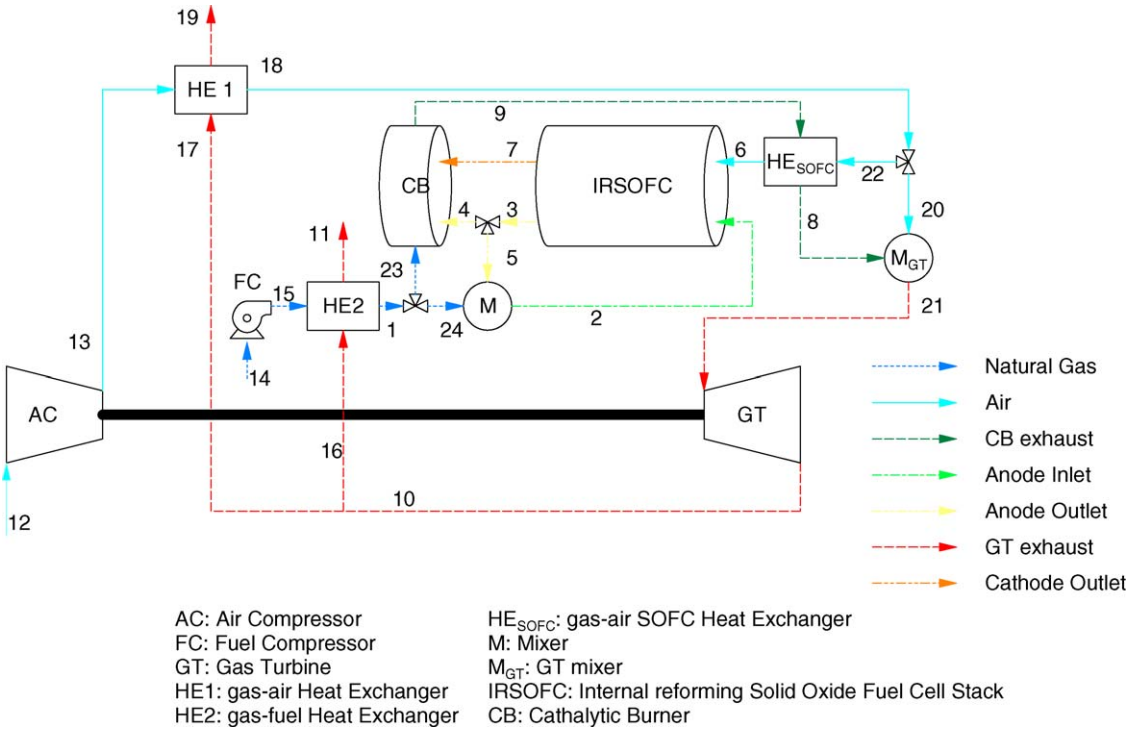

Fig. 1. Plant layout.

The working principle of the plant can be summarized as follows. Air and fuel are pressurized at the fuel cell operating pressure. The air compressor mechanical work is supplied directly by the gas turbine. Air (state-point 13) and fuel (state-point 15) are preheated before entering the SOFC stack by means of the two heat exchangers. These last ones are designed to transfer the outlet GT heat flow rate (state-point 10) to the inlet air and fuel streams. Air (state-point 6) and fuel (state-point 1) streams are fed, respectively, to the cathode and anode compartment of the fuel cell. In the anode compartment, fuel is mixed with anode re-circulated stream (state-point 5). Then, it is carried to external surface of the SOFC tubes (state-point 2) where the internal reforming reactions occur, releasing hydrogen, which is brought to the three phases boundary (TPB) [1–5] sites where the anode semireactions occur. Air is fed to the top of the stack (state-point 22) where is further preheated and finally carried, by an inner injection tube, into the SOFC tube (state-point 6). There it participates at cathode electrochemical semireaction. In this way ions O^{2-} pass through the electrolyte and electrons are conducted into the external circuit, determining the required dc electricity, which is converted in a more suitable ac power by using a proper inverter. Finally, anode outlet stream (state-point 3) is partly re-circulated (state-point 5), as mentioned above, and partly (state-point 4) meets the depleted air coming from the SOFC tubes (state-point 7). The air and the unreacted fuels of the anode stream are burnt within the catalytic burner partly increasing the stream temperature and partly preheating the inlet air (state-point 22). The combustor outlet stream temperature and pressure (state-point 9) is suitable to enter the gas turbine. The GT produces mechanical work for air and fuel compressors and the directly coupled electrical generator. In this way, it is possible to cover all the passive loads of the plant and supply additional ac (or eventually dc power) for the user. A proper mixer is placed before GT inlet in order to control its inlet temperature. Finally, after preheating air and fuel, GT exhaust stream (state-point 10) can be used to produce a medium temperature heat flow rate, recovering thermal energy from the plant. Even if its temperature is usually not high enough to produce steam, it can be easily used for

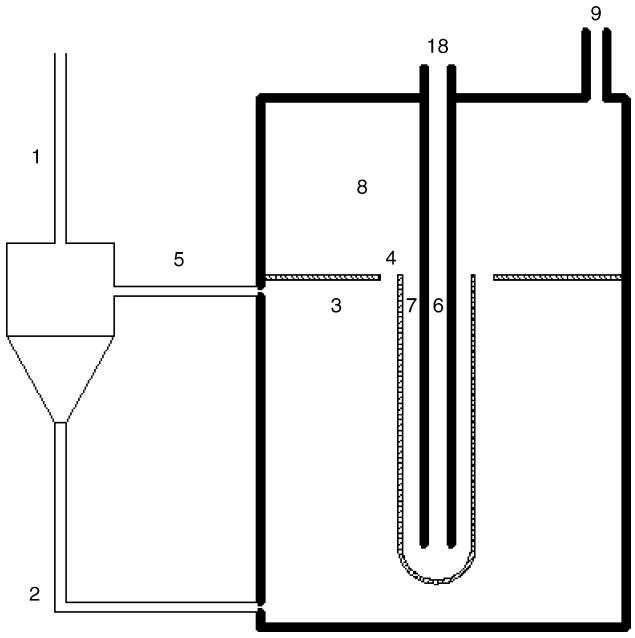

Fig. 2. SOFC stack with anode re-circulation arrangement.

space and water heating, providing additional efficiency to the plant.

Air compressor and gas turbine are assumed to be coupled on the same rigid shaft; fuel compressor, much smaller than all the other turbomachineries, is assumed to change its rotor speed arbitrary. As a consequence, fuel pressure ratio might be higher than air one, or vice versa. In this case it is necessary to laminate the highest pressure stream, before entering the cell. The high operating temperature of the cell and its structural peculiarities make mandatory to avoid excessive pressure gradients through the cell.

3. Part-load strategy approach

The above-mentioned hybrid system is investigated by authors in previous works, dealing with both I and II laws analysis [13–15]. Results showed that, at full-load, this plant could reach a net electrical efficiencies close to 70%. The aim of the paper is to investigate the performance and inefficiencies of this plant during partial load. The investigation of the part-load operation is very complex since many solutions, returned by the simulation code, must be rejected since physically infeasible. In fact:

(1) Turbomachineries, simulated on the basis of their maps, operate only in a very small range of mass flow rate, pressure ratio and rotor speed. Maps are very sensitive to the variation of design and operating parameters: small changes to the code input parameters often correspond to a turbomachinery operating point placed outside its map, i.e. an infeasible solution.
(2) Some set of input parameters may correspond to a negative net mechanical work of the AC–GT group. Here no external motor is introduced in order to supply additional mechanical work to the AC–GT. As a consequence, the solution is rejected.
(3) The GT pressure ratio might be higher than air compressor one, determining a virtual outlet GT pressure lower than the environmental one. The solution is rejected in this case too.
(4) The SOFC operating temperature and the GT inlet temperature cannot exceed upper bounds, due to their technological constraints. Thus, in case the code returned values of such temperatures higher then their respective limits, such mathematical solution is rejected.

Previous papers introduced a part-load operation strategy based on GT variable speed control [9,10]. Here, this choice is avoided. In fact, the use of a variable speed control is very complex and sometimes inefficient, since: (i) the GT inlet conditions depend dramatically on SOFC performances, varying as a consequence of changes in its operational and design parameters. The GT map is also very sensitive to its inlet conditions and to its mass flow rates. Thus, in case of high load excursion GT map dramatically changes, so that it is impossible to find a coupling point with the air compressor whatever rotor speed is selected; (ii) the managing of a variable speed control system is usually very complex, versus the needs for simplicity and safety required for the part-load operation of these hybrid plants.

Here, the quasi-stationary assumption is employed. As a consequence, only gradual load excursion are taken into account. The modeling of rapid load excursion or of the start-up would require a more detailed transient model of all the component of the plant. These events are very rare since plant structural constraints must be considered: it is not possible to rapidly change cell temperature and pressure since this variation would dramatically damage cell tubes. The start-up occurs only when the system is started, and can be summarized as follows: SOFC stack is bypassed and fuel is channeled to the combustor; its exhaust gas gradually increase stack temperature and are expanded into the GT. Turbomachineries speed is gradually increased up to its design value. Then steam is produced by the external boiler and mixed with fuel before entering the stack and the reforming process is started. Then, when the reforming reaction is fully activated, the electrochemical reaction can occur generating the steam required for the reforming reaction. Finally, when the steam to carbon ratio (r_{SC}) approaches the required value, the external boiler is disconnected, and the plant is ready to produce electricity and steam.

4. Thermodynamic chemical and electrochemical model

The calculation of state-points thermodynamic in the plant properties is very complex since: (i) almost all chemical, physical and electrochemical phenomena are governed by strongly non linear equations; (ii) the hybrid SOFC–GT plant under investigation is a very highly coupled system.

In the present paper, in order to simulate the above-mentioned phenomena, a zero-dimensional model is implemented. This approach is promised to be very effective since represents the best compromise between computational time and content of information [9–19]. The model, considered in this work, is based on the following general assumptions: (i) all the inlet and outlet sections flows are one-dimensional; (ii) thermodynamic equilibrium; (iii) steady state; (iv) no heat losses towards the environment; (v) negligible kinetic and gravitational terms in the balance equations.

The simulation code is written in MATLAB and implemented with a proper graphical user interface. It consists of several subroutines, each one is designed in order to calculate: fluid thermodynamic properties, components energy exchanges, electrochemical performances, etc.

5. Fluid thermodynamic properties

Although solid oxide fuel cells can be fed by a number of fuels (methane, natural gas, biogas, syngas, etc.), in this paper the use of natural gas is considered [13,14]. It basically consists of N_2 and CH_4 (Table 1). Furthermore, it is assumed the use of air (21% O_2 and 79% N_2) as oxidant [13,14].

In the thermodynamic processes considered in the plant, temperature and pressure range, respectively, from 25 to 1300 °C and from 1.00 to 10 bar. The assumption of ideal gas is considered for all the gases. The water properties are calculated on the

Table 1
Typical composition of Italian natural gas ($\times 10^2$ mol mol^{-1})

CH_4	99.728
Ethane	0.0006
Propane	0.0148
Isobutane	0.007
Butane	0.0019
Isopentane	0.0022
Pentane	0.00001
Hexanes	0.0078
N_2	0.207
CO_2	0.0311

basis of the superheated steam model, based on IAPWS-IF97 equations [13,14]. In all the range of temperature and pressure considered, the Dalton's law (ideal mixtures) is adopted. For all the substances, a temperature-dependent specific heat model is adopted:

$$c_{p,i} = \frac{\tilde{R}}{M_i}(A + BT + CT^2 + DT^{-2}) \quad (1)$$

The coefficients of Eq. (1) are reported in Table 2.

Suitable codes are developed in order to calculate specific enthalpy, entropy, chemical and physical exergy, on the basis of temperature, pressure and chemical composition. The developed software also allows the calculation of mixture temperature starting from its chemical composition, pressure and enthalpy (or entropy). This calculation is performed iteratively using the MATLAB optimization toolbox. Specific chemical exergy is also required for the exergy balances in the mixers and in the chemical (or electrochemical) reacting devices. This property is calculated on the basis of its definition [20]:

$$\dot{ex}_{ch} = \left(\sum_{i=1}^{7} \dot{n}_i\right) \sum_{i=1}^{7} (x_i \, \widetilde{ex}_{ch,i} + \tilde{R} T_a x_i \ln(x_i)) \quad (2)$$

where $\dot{ex}_{ch}$ is the reference specific chemical exergies [20] reported in Table 3. The present model also allows the calculation of pressure drops through the plant components. This calculation is performed on the basis of a simplified approach [10] i.e. assuming constant friction factor and avoiding the calculation of mixture viscosity. Consequently, pressure drops are evaluated only on the basis of fluid density and mass flow rate [10].

Table 2
Specific heat capacity constants

	A_i	B_i (K^{-1})	C_i (K^{-2})	D_i (K^2)
H_2O	3.47	1.45E−03	0	1.21E+03
CO	3.376	5.57E−04	0	−3.10E+03
H_2	3.3249	4.22E−04	0	8.30E+03
O_2	3.639	5.06E−04	0	−2.27E+04
N_2	3.28	5.93E−04	0	4.00E+03
CO_2	5.457	1.05E−03	0	−1.16E+05
CH_4	1.702	9.08E−03	−2.16E−06	0

Table 3
Reference specific chemical exergy (kJ kmol^{-1})

H_2O	11710
CO	275430
H_2	238490
O_2	3970
N_2	720
CO_2	20140
CH_4	836510

6. Electrochemical model

SOFC are claimed to be able to electrochemically oxidize not only hydrogen but also carbon monoxide [1,2], which would be available for the electrochemical reaction by the anode recirculated stream and by the products of pre-reforming reaction [1,2]. Presently, it is not clear the real mechanism that is responsible for CO consumption within the anode compartment of the fuel cell. Even if the electrochemical reaction of CO is theoretically possible, it must be taken into account that, at the anode compartment of the SOFC, the shift reaction also occurs, converting CO into hydrogen [1,2]. For the sake of simplicity, it is assumed that CO consumption occurs only due to the shift reaction, neglecting the electrochemical CO oxidation [9–15]. Consequently, anode and cathode semireactions can be summarized as follows:

$$H_2 + O^{2-} \rightarrow H_2O + 2e^- \quad (3)$$

$$\tfrac{1}{2}O_2 + 2e^- \rightarrow O^{2-} \quad (4)$$

$$H_2 + \tfrac{1}{2}O_2 \rightarrow H_2O \quad (5)$$

The overall electrochemical process is significantly exothermic. Even if part of the available heat it is utilized by the endothermic reforming process, it is mandatory to operate with high air to fuel ratios in order to reduce the stack temperature [1,2].

A detailed calculation of the electrochemical performance of the SOFC requires at least a mono-dimensional steady model, since all the main parameters (i.e. temperature, pressure, voltage, current density, i, etc.) vary along the tube axis [9–15]. In order to reach a good compromise between calculation accuracy and computational effort, a zero-dimensional model is adopted. In fact, the gradients of thermodynamic and electrochemical properties are usually not remarkable along the tube axis. In addition, the outlet radial temperature gradients are always negligible [19]. As a consequence, all SOFC parameters are evaluated at the outlet temperature, pressure and chemical composition [19].

The electrochemical performance of a fuel cell depends on several parameters, namely: (i) the inlet anode and cathode streams chemical composition; (ii) their mass flow rates, temperatures and pressures; (iii) the SOFC materials and its geometry; (iv) the SOFC components thickness; (v) the current density; (vi) the fuel utilization factor. The electrochemical performance is usually described by the polarization curve obtained by plotting the voltage versus the current density [2]. In such diagram the maximum theoretical reversible voltage and the overall losses, as a function of the current density, are shown. In general, the

fuel cell achieves its maximum reversible voltage in case of no current required by the external load [2]. The calculation of such voltage is performed on the basis of a simple charge balance and on the Nerst equation:

$$E = \frac{\Delta G_f^\circ}{2F} + \frac{\tilde{R}T}{2F} \log\left(\frac{p_{H_2}\sqrt[2]{p_{O_2}}}{p_{H_2O}}\right) \quad (6)$$

Note that the Gibbs free energy, at standard pressure, depends dramatically on temperature. This function is calculated taking into account the ideal gas mixture model and the empirical correlations for specific heats. Although the open circuit reversible voltage decreases when temperature increases, the real voltage shows the opposite trend since overvoltages must be taken into account. Thus, when electrons flow through the internal and external SOFC circuit some losses must be taken into account, decreasing cell voltage. These losses are mainly due to: (i) electrochemical reaction activation, V_{act}; (ii) circuits ohmic resistance, V_{ohm}; (iii) concentration V_{conc} (described in the following). In this simulation, overvoltages due to fuel and electrons crossover through electrolyte are neglected [9–19]. Consequently, the overall cell voltage is calculated as follows:

$$V = E - V_{ohm} - V_{act} - V_{conc} \quad (7)$$

Presently, literature data for validating the electrochemical model are still scarcely available [2]. Thus, all the overvoltage models cannot be easily validated. Despite, the overall model result (i.e. the polarization curve) can be compared with experimental ones in order to evaluate the global model accuracy. The considered model is validated on the basis of literature data [19]. Polarization curves, plotted on the basis of the following model, are displayed in Figs. 3 and 4.

7. Activation overvoltage

Kinetics of electrochemical reactions are measured by the current density. This is the ratio between the overall current required by the external load and active SOFC area [1–5]. Both anode and cathode semireactions must be "catalyzed", supplying some additional energy in order to speed up the overall electrochemical reaction [2]. This energy, i.e. the activation energy, is usually measured by the overpotential, which is the difference between equilibrium and non-equilibrium voltage [1].

The activation overvoltage is calculated using the Butler–Volmer equation [13,14]:

$$i = i_0\left[\exp\left(\alpha\frac{n_e F}{RT_s}V_{act}\right) - \exp\left(-(1-\alpha)\frac{n_e F}{RT_s}V_{act}\right)\right] \quad (8)$$

The calculation of the activation overvoltage must be performed iteratively since it is not possible to reverse the Butler–Volmer equation. This circumstance is very expensive about the computational point of view but allows to avoid the typical errors yielded by the Tafel equation [2] at current densities lower than the exchange ones. The exchange current densities could not be handled as constant, since they are dramatically dependent on SOFC operating temperature [9]. The charge transfer coefficient, α, is assumed constant at 0.50 [2].

The activation overvoltage depends on the exchange current density, since this parameter is a measurement of electrochemical kinetics. For any equilibrium redox reaction, the cathodic current density is balanced by the anodic one. which is called the exchange current density [2]. Unfortunately, its calculation and measurement is usually very complex. Some authors predicted the value of the exchange current density by means of semi-empirical correlations [9]. In case of SOFC, the following

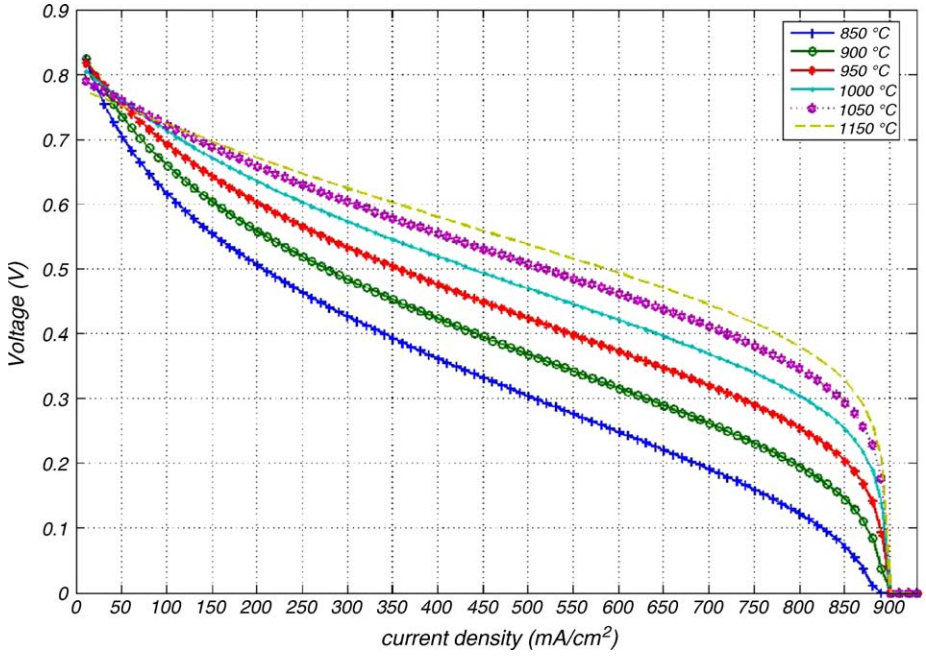

Fig. 3. Polarization curves, varying the operating temperature, $p = 1.00$ bar.

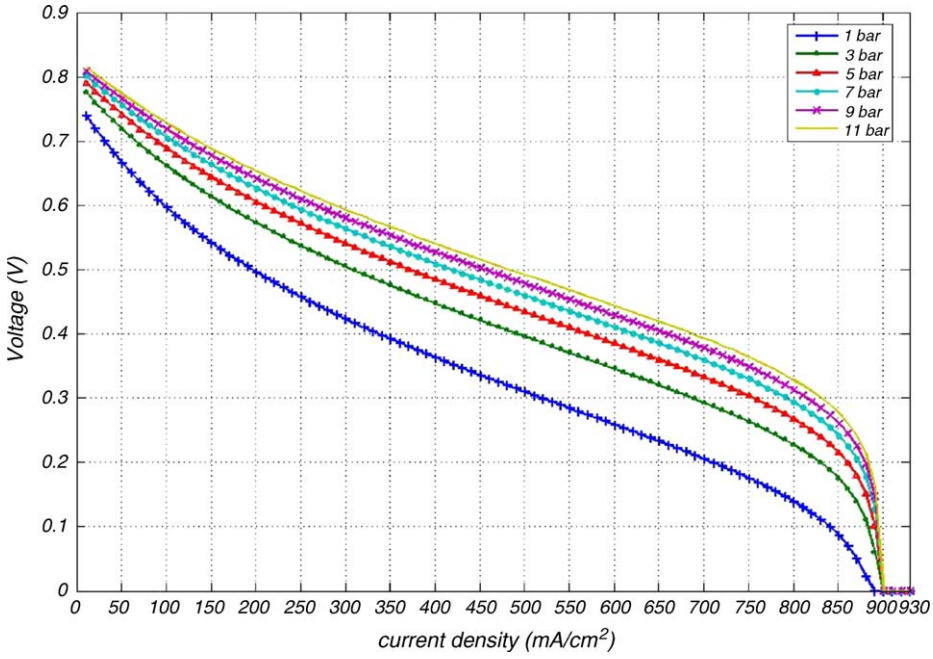

Fig. 4. Polarization curves, varying the operating pressure, $t = 1000\,^{\circ}\mathrm{C}$.

correlations are considered:

$$i_{0,\mathrm{anode}} = \gamma_{\mathrm{anode}} \left(\frac{p_{\mathrm{H_2}}}{p_{\mathrm{ref}}}\right) \left(\frac{p_{\mathrm{H_2O}}}{p_{\mathrm{ref}}}\right) \exp\left(-\frac{E_{\mathrm{act,anode}}}{RT_{\mathrm{s}}}\right) \quad (9)$$

$$i_{0,\mathrm{cathode}} = \gamma_{\mathrm{cathde}} \left(\frac{p_{\mathrm{O_2}}}{p_{\mathrm{ref}}}\right)^{0.25} \exp\left(-\frac{E_{\mathrm{act,cathode}}}{RT_{\mathrm{s}}}\right) \quad (10)$$

The activation overvoltage curves are displayed in Fig. 5, as a function of the SOFC operating temperature. Obviously, such losses can be reduced increasing cell operating temperature or lowering its operating current density.

8. Ohmic losses

The SOFC operating temperature is high in order to reduce its ohmic losses [1–5]. This overvoltage is due to: (i) the electrons flow through the anode, cathode and interconnections; (ii) the ionic flow through the electrolyte. The SOFC material resistivity is a temperature-dependent function [2]. Usually, the SOFC ohmic resistance is due mostly to the interconnections. Presently, like almost all the papers, the ohmic losses are simulate by means of resistivity, obtained by the experimental temperature-dependent correlations [13,14]. Such resistances are summated assuming a series electrical scheme. In this way, the ohmic loss is calculated as follows:

$$V_{\mathrm{ohm}} = ir \quad (11)$$

$$r = \delta\rho \quad (12)$$

$$\rho = A \exp\left(\frac{B}{T}\right) \quad (13)$$

For the considered air electrode supported SOFC (Ni-YSZ), the coefficients A and B of resistivity (Eq. (13)) and the components thickness, δ (in Eq. (12)), are reported in Table 4 [13,14]. Ohmic overvoltage curves are displayed in Fig. 5.

Table 4
SOFC resistivity constants

	A (Ω cm)	B (K)	δ (cm)
Anode	0.00298	1392	0.01
Cathode	0.00814	−600	0.19
Electrolyte	0.00294	−10350	0.004
Interconnections	0.1256	−4690	0.0085

9. Concentration overvoltage

Anode electrochemical semireaction causes the hydrogen consumption at the electrode–electrolyte interface. The H_2 partial pressure decreases when it is not readily replenished from the fresh fuel. The decrease of this partial pressure reduces cell voltage because of the Nerst equation [2]. Similarly, the same phenomenon occurs at the cathode compartment where oxygen is consumed by the cathode electrochemical semireaction. The concentration overvoltage can be calculated taking into account transportation phenomena occurring in the fuel cell [2]. This overvoltage is usually negligible for low current density [1,2]. Concentration is usually simulated neglecting heat convection and taking into account only diffusion phenomena, introducing binary and Knudsen diffusion models [19]. Previous papers, based on such models, showed that the resulting limiting current density is only slightly dependent on the SOFC temperature [19]. Thus, in this simulation, the overall concentration overvoltage calculation is simplified assuming a constant value for the limiting current density and implementing the Fick's law [13,14]. Finally, the concentration overvoltage can be

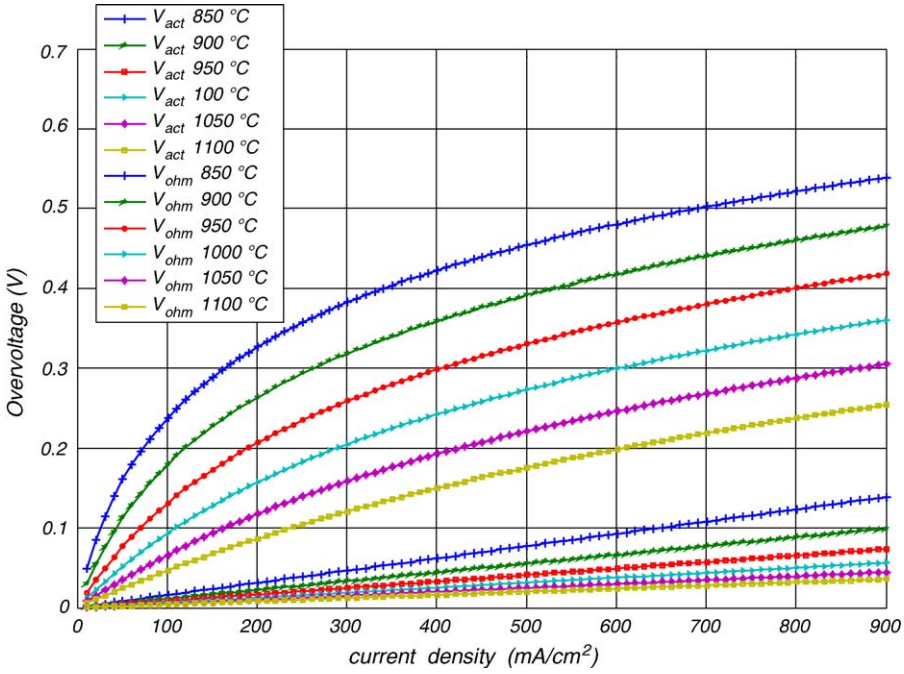

Fig. 5. Activation and ohmic overvoltages, varying the operating temperature, $p = 1.00$ bar.

evaluated as

$$\Delta V_{\text{conc}} = \frac{RT}{2F} \ln\left(1 - \frac{i}{i_l}\right) \tag{14}$$

The simulation of concentration overvoltage, based on the above-mentioned model, is shown in Fig. 6.

10. Internal reforming model

The above discussed electrochemical reaction deals with hydrogen as fuel. Here, the fuel cell is fed by methane. The usual high operating temperature of SOFC allows to sustain the reforming process within the anode compartment of the stack [1–5], which covered by a suitable catalyst for the reforming reaction, can convert almost all the methane into hydrogen. The considered reforming reactions are:

$$CH_4 + H_2O \rightarrow CO + 3H_2 \tag{15}$$

$$CO + H_2O \leftrightarrow CO_2 + H_2 \tag{16}$$

From these equations, it is clear that this process requires steam. This can be produced externally by a boiler or by a heat recovery steam generator supplied by the gas turbine exhaust gases, that represent an additional capital cost. For this reason, it is assumed to supply the required steam by recirculating the anode outlet one [9,10]. This process can be performed by means of an ejector, according to the scheme displayed in Fig. 2. The fresh fuel (state-point 1, Fig. 2), coming from the heat exchanger, is mixed with the anode re-circulated stream (state-point 5), within a device that operates simultaneously as a mixer and as a pre-reformer. Air, coming from the heat exchanger, is preheated by a virtual counterflow heat exchanger, within the SOFC air injection tube. Then, it is brought to the bottom of the SOFC tube where it can participate at the cathode electrochemical semireaction. Finally, depleted air and unreacted fuel are combusted in a catalytic burner (Fig. 2). In order to simulate both combustion and heat exchange phenomena occurring on the top of the fuel cell stack, it is assumed that the combustion and heat exchange processes are in sequence.

Assuming the reforming reactions at chemical equilibrium, their reaction rates can be calculated by using the definitions of the equilibrium constants and the fuel utilization factor. Furthermore, the rate of anode re-circulation is calculated in order to reach the desired value of the steam to carbon ratio, r_{SC} [2] which must be sufficiently high in order to avoid carbon deposition [1,2].

The IRSOFC subroutine allows to calculate SOFC outlet stream chemical composition once that inlet mass flow rates, temperature and pressure are fixed. This calculation requires the stack equilibrium temperature too. The temperature is iteratively calculated by means of the energy balance on the SOFC stack.

To solve the reforming process an algebraic system of equations is suitably developed. It is obtained handling mole balances and: (i) fuel utilization factor, U_f; (ii) constant of reactions, K; (iii) recirculation rate, r:

$$K_{\text{reforming}} = \frac{x_{H_2}{}^3 x_{CO}}{x_{H_2O} x_{CH_4}} \left(\frac{p_3}{p^0}\right)^2 = \frac{(\dot{n}_{H_2,1} + 3x + y - z)^3 (\dot{n}_{CO,1} + x - y)}{(\dot{n}_{H_2O,1} - x - y + z)(\dot{n}_{CH_4,1} - x)(\dot{n}_{tot,1} + 2x)^2} \times \left(\frac{p_3}{p^0}\right)^2 \tag{17}$$

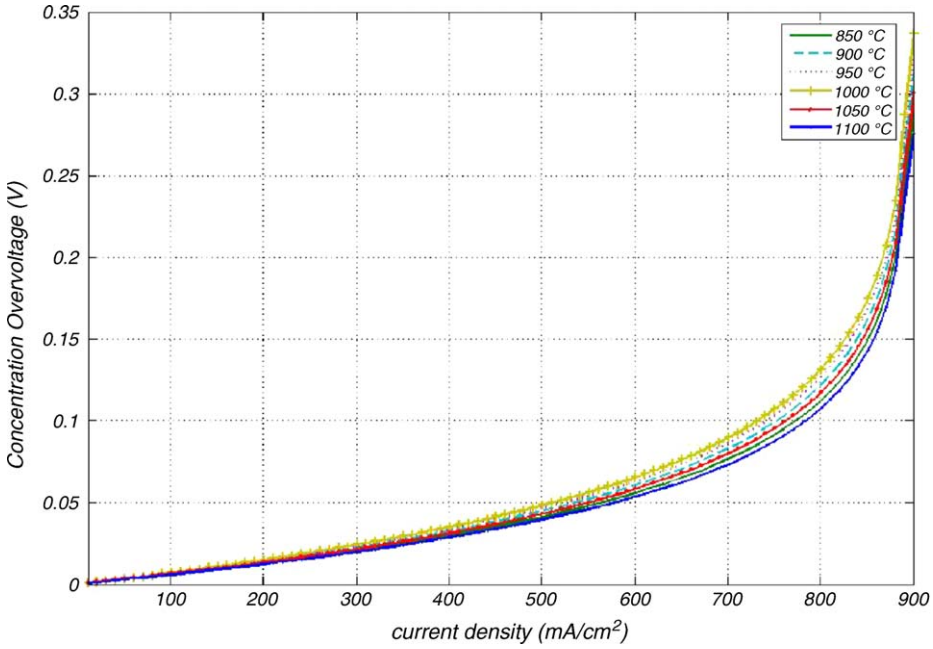

Fig. 6. Concentration overvoltage, varying the operating temperature, $p = 1.00$ bar.

$$K_{\text{shift}} = \frac{x_{H_2} x_{CO_2}}{x_{H_2O} x_{CO}} = \frac{(\dot{n}_{H_2,1} + 3x + y - z)(\dot{n}_{CO_2} + y)}{(\dot{n}_{H_2O,1} - x - y + z)(\dot{n}_{CO} + x - y)} \tag{18}$$

$$z = \frac{U_f(\dot{n}_{H_2,1} + 4\dot{n}_{CH_4,1} + \dot{n}_{CO,1})}{1 - r(1 - U_f)} \tag{19}$$

$$r_{SC} = \frac{\dot{n}_{H_2O,2}}{\dot{n}_{CH_4,2}} \Rightarrow r = \frac{r_{SC}\dot{n}_{CH_4,1} - \dot{n}_{H_2O,1}}{z - y + x(r_{SC} - 1)} \tag{20}$$

The above displayed reaction constants depend only on SOFC operating temperature, as shown in Fig. 7. Suitable subroutines are developed in order to evaluate whatever constant of reaction, based on temperature-dependent enthalpy and Gibbs functions.

The solution of the above-mentioned system of algebraic equations allows one to evaluate also the value of the electrical power produced by the SOFC stack. Thus, recalling the subroutine calculating cell potential, the SOFC electrical power production is evaluated on the basis of a simple mole and charge balance:

$$P = 2FzV \tag{21}$$

The use of this equation is possible since the total current is the sum of all the singular cell currents. An inverter is employed in order to match the user's requests, in terms of current and voltage [13–19]. The inverter efficiency, at design and partial load, is simulated on the basis of semi empirical functions depending on the net electrical power [10].

11. Combustor model

Anode outlet stream chemical exergy rate is relatively high since not all the fuel is consumed by the cell. SOFC outlet hydrogen molar fraction is not negligible, since the fuel utilization factor, is usually lower than 85% [1,2]. In the combustor, the fuels available are: hydrogen and in lower percentages carbon monoxide and methane. The oxidant is the depleted oxygen of the cathode outlet stream. As mentioned above, the air mass flow rate is much higher than the fuel one in order to control stack temperature. Consequently, oxygen mass flow rate is much higher than the required combustion stoichiometric value. Combustion reactions, assumed at chemical equilibrium and driven into completion, are:

$$CH_4 + 2O_2 \rightarrow CO_2 + 2H_2O \tag{22}$$

$$H_2 + \tfrac{1}{2}O_2 \rightarrow H_2O \tag{23}$$

$$CO + \tfrac{1}{2}O_2 \rightarrow CO_2 \tag{24}$$

Combustor outlet temperature is calculated on the basis of a simple energy balance on the combustor control volume. The calculation of combustor exergy destruction rate requires the evaluation of inlet and outlet chemical exergy flows too.

12. Heat exchanger model

Tubular SOFC operating temperature must be close to 1000 °C in order to make more effective the electrolyte performance [1,2]. Although the overall chemical and electrochemical reactions are largely exothermic, air and fuel must be preheated before entering the stack in order to avoid high temperature gradients [2]. Such processes are performed by means of two tubes in tube counterflow heat exchangers. These devices are simulated on the basis of the ε-NTU method [21,22], implementing temperature-dependent specific heats. Some additional assumptions are considered: (i) constant global heat transfer coefficient; (ii) enthalpy independent from pressure. Heat exchange area, inlet flows temperature and pressures are input

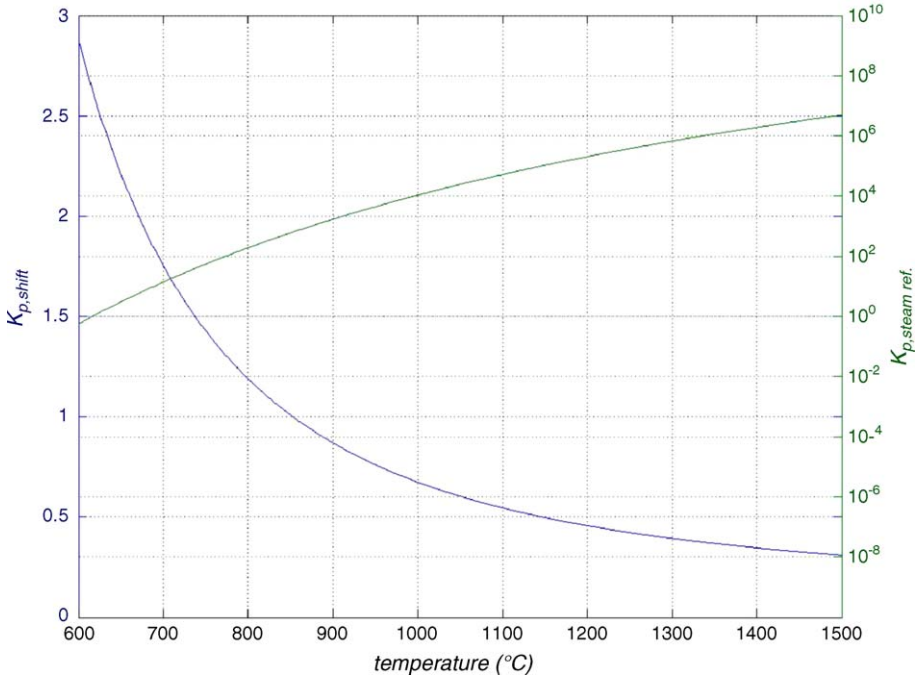

Fig. 7. Constants of reforming and shift reactions.

data. An iterative procedure is implemented in order to assess the outlet temperatures, based on the calculation of average hot and cold fluids specific heats. These parameters depend on the unknown HE outlet temperatures. Thus, guess values for such temperatures are selected, allowing the calculation of the average specific heats and consequently, by means of the ε-NTU method, the outlet temperatures are re-calculated. The procedure is stopped when the convergence criterion on such temperatures is satisfied. Finally entropy and exergy balances can be performed in order to calculate HE exergy destruction rate.

13. Mixer model

The mixer is the simplest device of the plant. It is necessary in the fuel cell stack and at GT inlet in order to control its inlet temperature. The mixer model is based on mass, moles, energy and exergy balances. Note that its exergy destruction rate depends on variations of both physical and chemical exergy flows.

14. Turbomachineries model

Three turbomachineries are included in the plant under study: air compressor, fuel compressor and gas turbine. These devices are investigated in detail, in order to match their requirements with those coming from the fuel cell. Maps, available in the archives of software GSP and Gasturb, are used, describing the mass flow rate versus pressure ratio curves, for different values of rotor speed. Since no map matched the values of mass flow rate and pressure ratios required by the components of the plant under investigation, all these maps are properly scaled. In particular, a centrifugal compressor (based on ASME 95-GT-79 map) and a radial turbine (based on NASA-CR-174646 map) are selected. Such devices show large ranges for both mass flow rate and pressure ratios, allowing the working points moving in the feasible region of these maps. Axial turbines, for example, can work only very close to the design mass flow rate so that it is very difficult to find a real working point in case of partial load. All these maps are corrected on the basis of the values of inlet temperature and pressure:

$$\dot{m}_{\text{correct}} = \dot{m} \frac{\sqrt{\frac{T_{\text{inlet}}}{T_{\text{ref}}}}}{\frac{p_{\text{inlet}}}{p_{\text{ref}}}} \tag{25}$$

$$N_{\text{correct}} = \frac{N}{\sqrt{\frac{T_{\text{inlet}}}{T_{\text{ref}}}}} \tag{26}$$

The scaled correct maps of the air compressor, fuel compressor and gas turbine are displayed, respectively, in Figs. 8–10. In case of air or fuel compressor, the inlet status corresponds at the environmental one, whereas temperature and pressure of the GT inlet stream can considerably vary according to the changes in the design and operating parameters. Consequently, once the GT corrected map is fixed, the un-corrected changes at each iteration of the procedure. Air compressor and gas turbine are assumed to be coupled on a unique shaft; as a consequence, they must have the same rotor speed, whereas the speed of the fuel compressor can vary independently. The maps are used to calculate isentropic efficiencies and pressure ratios, as a function of mass flow rates, rotor speed and inlet conditions. Thus, the outlet conditions of the components are calculated, as well as energy, entropy and exergy balances. The use of maps restrict dramatically the feasible working region of the plant: whenever the working point of a turbomachinery falls outside the map or

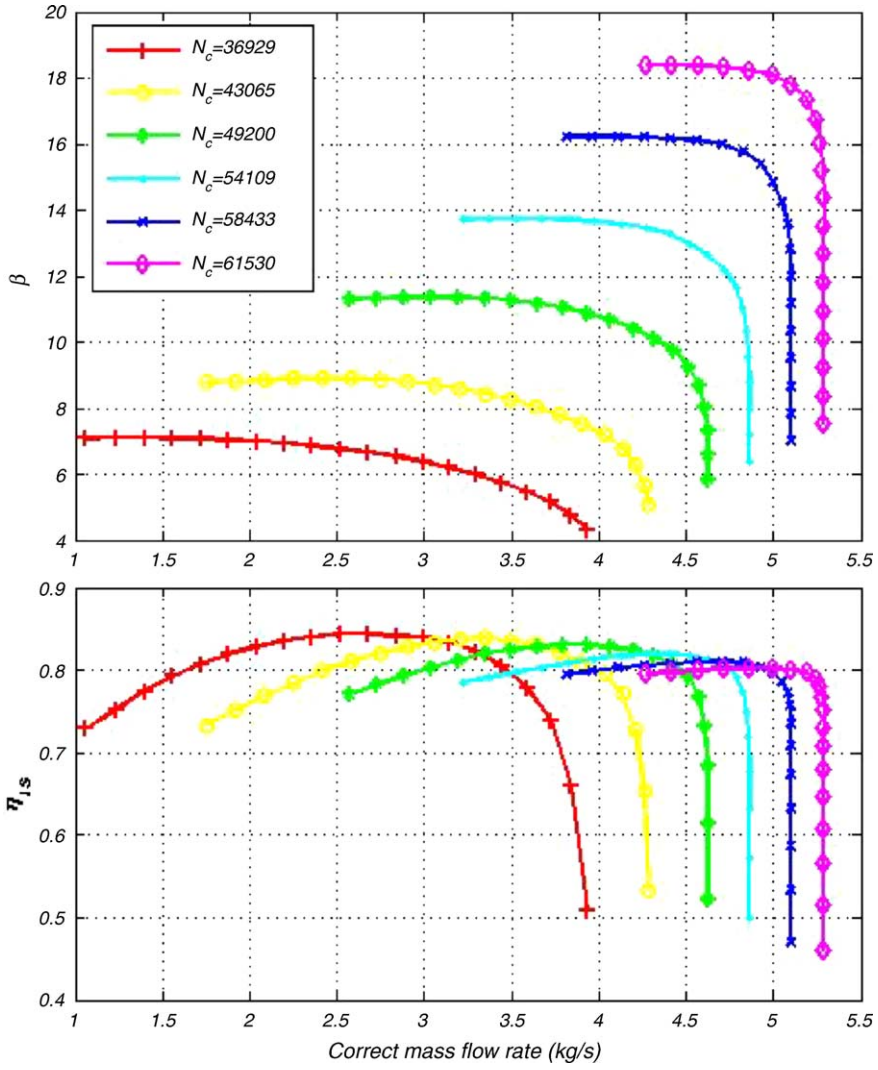

Fig. 8. Centrifugal air compressor correct map.

the GT outlet pressure calculated is lower than the environmental one, the solution is rejected. The overall mechanical power produced by turbomachineries is

$$L_{\text{net}} = (L_{\text{GT}} - L_{\text{AC}})\eta_{\text{EG}} - L_{\text{FC}} \tag{27}$$

The efficiency of the electrical generator, at deign and partial load, is simulated on the basis of semi-empirical functions [10].

15. Plant model

The code is developed sequentially, avoiding the solution of large strongly non-linear algebraic system. Each system device is simulated by a suitable subroutine. Despite of this effort, many internal loops are required as a consequence of the physical and logical relationships existing among plant components. The overall simplified flow chart is shown in Fig. 11. Once all these setting/operational parameters are assigned, the code simulates both air and fuel compressors with the following steps: (i) reading the turbomachineries maps, implemented in the code; (ii) calculating outlet pressure and isentropic efficiency by the above-mentioned maps; (iii) recalling the compressor subroutine, evaluating its outlet conditions and energy/exergy flows. The calculation of compressors allows the evaluation of pressures at each state-point of the plant. Then, a stack guess temperature is chosen in order to let the IRSOFC subroutine calculate the stack outlet chemical composition. A guess value of the temperature at the state-point 23 (Fig. 1) is fixed, allowing the call of combustor subroutine. An other guess value is fixed for temperature at state-point 18. Such a value allows to calculate sequentially the outlet thermodynamic properties of: (i) the SOFC counterflow heat exchanger; (ii) the GT mixer; (iii) the GT; (iv) the gas–air heat exchanger. The GT is simulated with the same procedure used for the air and fuel compressors. The calculation of gas–air heat exchanger allows to re-calculate temperature at state-point 18 and then evaluate the convergence criterion dealing with such temperature. Similarly, the calculation of gas–fuel heat exchanger and the energy balance on SOFC stack allows to apply the convergence criterion on temperatures of state-points 23 and 4. Finally, the code verifies if: (i) the overall GT/AC mechanical power is positive; (ii) the GT outlet pressure is higher than the environmental one. In case these

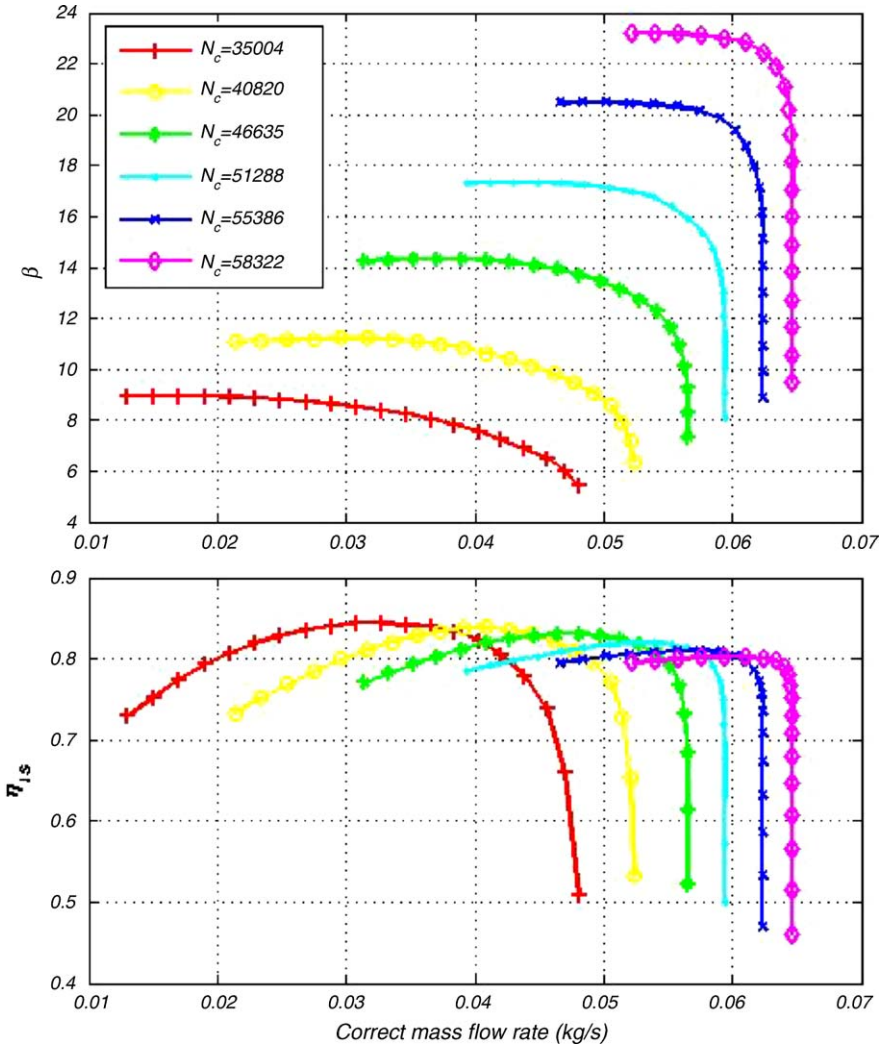

Fig. 9. Centrifugal fuel compressor correct map.

conditions are not matched, the solution is rejected. The post processing procedure allows to calculate state properties and operating parameters required by the user (chemical composition, physical and chemical exergy, entropy, enthalpy, density, thermal flow, mechanical flows, I and II law efficiencies, overvoltages, etc.).

16. Full-load simulation: results and discussion

The plant under investigation is simulated at full-load operation on the basis of the fixed setting parameters displayed in Table 5. Results are shown from Tables 6–8: the former displays some of the most interesting plant results, the second one shows devices energy/exergy flow rates, finally the last one displays some of the state-point thermodynamic properties. The steam to carbon ratio (r_{SC}) is set at 2.00. The fuel utilization factor is set at 80%: higher values are not recommended since high overvoltages would occur in the final section of SOFC tube. Furthermore, SOFC area is set in order to achieve high efficiencies. The resulting current density (194 mA cm^{-2}) is significantly low, allowing the cell to achieve a very high voltage (0.63 V versus 0.797 V, maximum theoretical reversible potential). Similarly, the remarkable values of *UA* for the preheating heat exchangers allow heat exchange efficiencies to achieve values higher than 90%. All the performance parameters are calculated by the simulation code. The most important ones are shown in Table 6. SOFC heat exchanger efficiency is relatively low as a consequence of its small exchange area. Higher efficiencies are not recommended in order to avoid significant temperature gradients in the cell. The overall electric stack efficiency is higher than 50%. In case of an ideal reversible cell, this efficiency could achieve a value higher than 72%. Turbomachineries, the inverter and the electrical generator operate at their design point achieving the maximum values of their efficiencies. The net overall result is an electrical efficiency higher than 65% and simultaneously a thermal efficiency close to 22%. Almost all the electrical power is produced by the fuel cell stack. The mechanical power produced by the GT is dramatically reduced by the work required to move compressors. Obviously, the thermal flow of the air heat exchanger is much higher than the fuel one since the air mass flow rate is two orders of magnitude higher than the fuel one. Inefficiencies lie mainly in those devices where

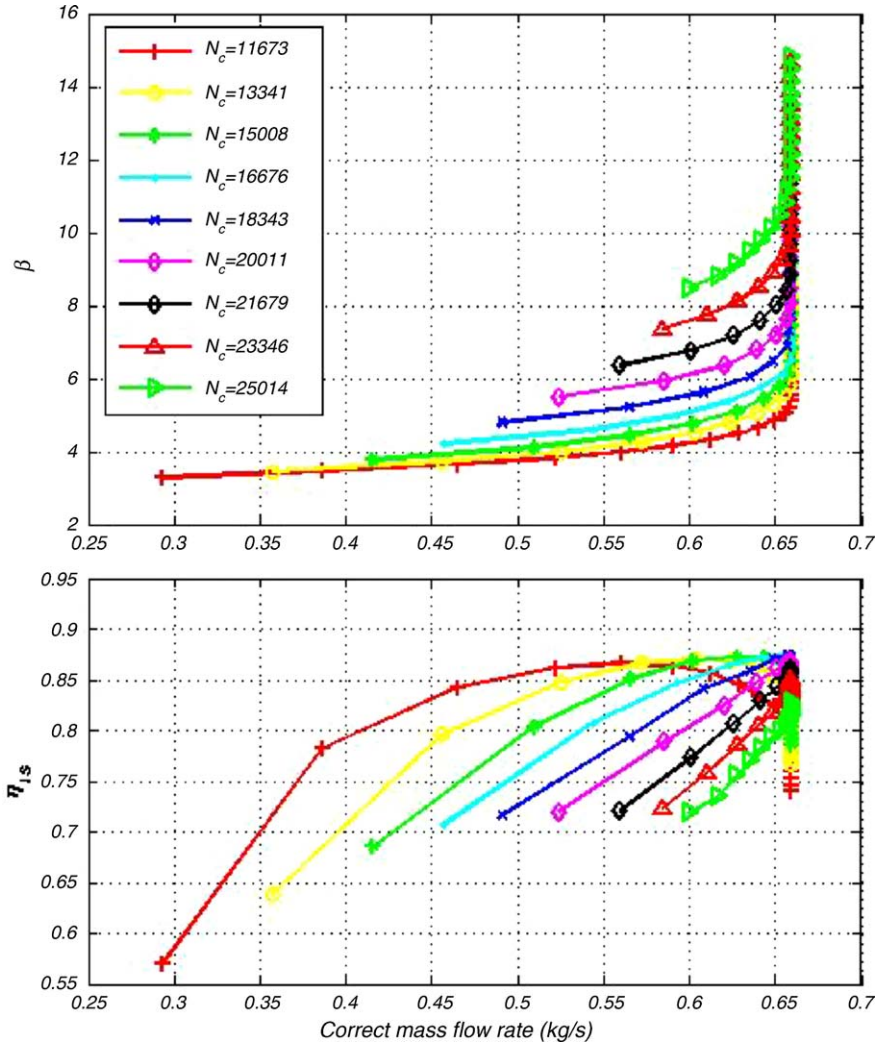

Fig. 10. Radial gas turbine correct map.

chemical processes occur. SOFC stack, where both reforming and electrochemical reaction occur, is the component where the highest efficiency defect (δ) is detected. Similarly the catalytic burner, site of combustion reactions, shows a remarkable exergy destruction rate. On the other hand, efficiency defects of turbomachineries are relatively low because of the high values of isentropic efficiencies (design point) and since their energy flows are less important in the overall plant balance. Finally, Table 8 shows some of the main thermodynamic properties of all the state-points of the plant. At design point outlet air and fuel compressors pressures are very close each other avoiding any lamination process. Furthermore, the SOFC temperature is close to the ideal value of 1000 °C and the calculated value of TIT is perfectly compatible with the present technological constraints imposed by GT technology. Obviously, the higher are pressure and temperature, the higher are the values of specific physical exergy. On the other hand, specific molar chemical exergy depends mainly on flow fuel content. This value, in fact, decreases (three orders of magnitude) after reforming, electrochemical and combustion reactions.

17. Partial load operation: results and discussion

The partial load operation of the plant could be managed handling the following parameters:

(1) air mass flow rate;
(2) fuel mass flow rate;
(3) combustor bypass, i.e. the ratio between the mass flow rate to the combustor and the mass flow rate going out from the gas–fuel heat exchanger;
(4) GT bypass, i.e. the ratio between the mass flow rate to the gas turbine mixer and the mass flow rate going out from the gas–air heat exchanger;
(5) AC–GT rotor speed (the speed of the electrical generator is changed using an inverter, according to user load request).

It is not possible to vary arbitrary all these operating parameters, since unfeasible solution would be achieved. In fact: (i) the turbomachineries operating points may fall outside of their map and (ii) the SOFC operating temperature may exceed the fixed

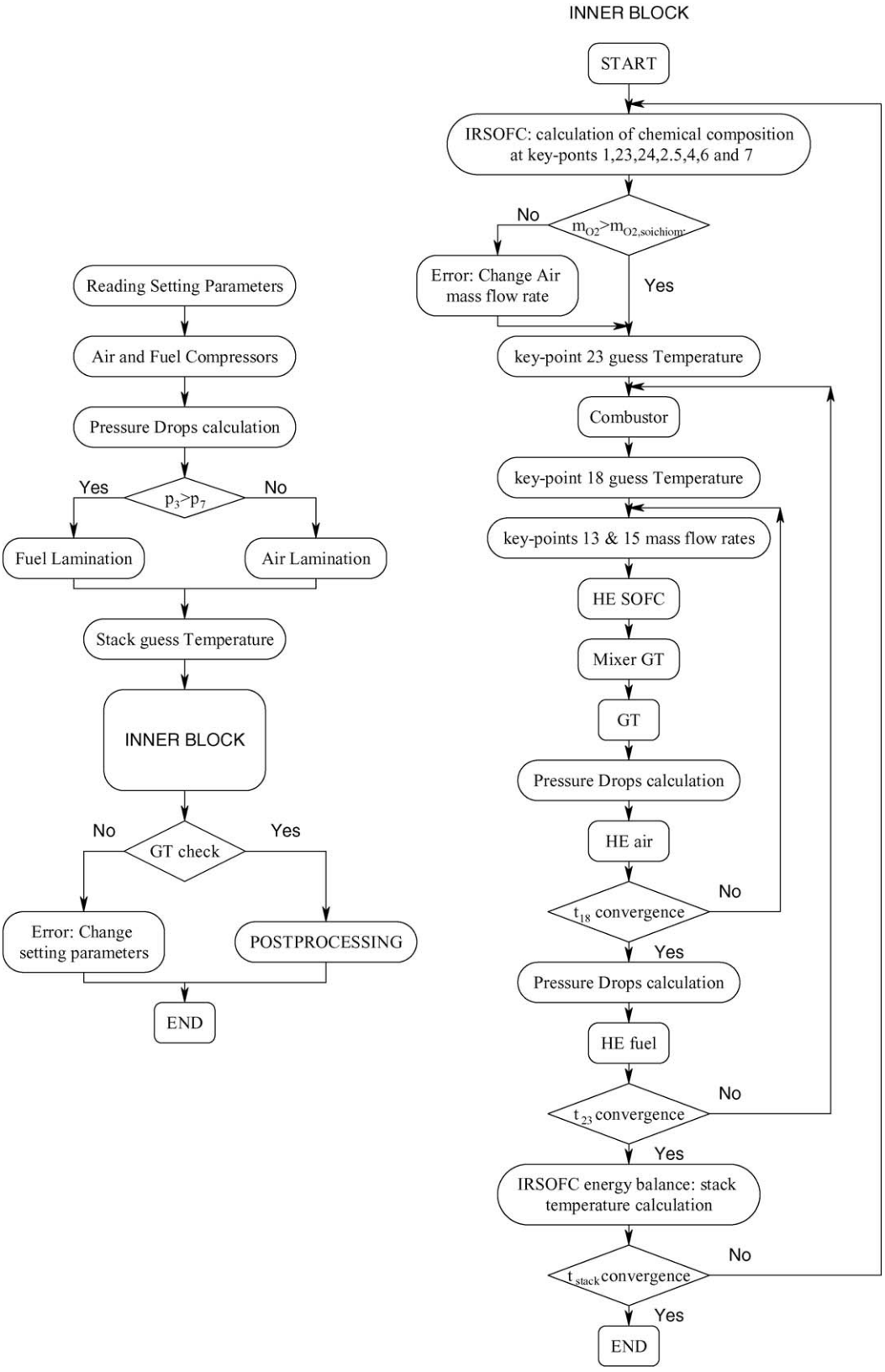

Fig. 11. Plant simulation simplified flow chart.

Table 5
Setting parameters

Parameter	Value
SOFC area (cm^2)	1.000E+07
r_{SC}	2.000E+00
U_f	8.000E−01
i_l ($mA\,cm^{-2}$)	9.000E+02
$t_{stack\,max}$ (°C)	1.250E+03
$\Delta p_{stack\,max}$ (bar)	6.000E−01
UA_{HE1} ($kW\,K^{-1}$)	1.500E+01
UA_{HE2} ($kW\,K^{-1}$)	1.650E−01
$UA_{HE_{SOFC}}$ ($kW\,K^{-1}$)	7.500E−01
Δp_{mixer} (%)	1.000E+00
Δp_{CB} (%)	4.000E+00
Δp_{stack} (%)	2.000E+00
$\eta_{inverter}$ (100%)	9.700E−01
$\eta_{inverter}$ (10%)	9.200E−01
$\eta_{electr.\,gen.}$ (100%)	9.500E−01
$\eta_{electr.\,gen.}$ (10%)	6.000E−01
η_{CB}	1.000E+00
m_{air} ($kg\,s^{-1}$)	1.885E+00
m_{fuel} ($kg\,s^{-1}$)	4.650E−02
t_{ref} (°C)	2.500E+01
p_{ref} (bar)	1.000E+00
$N_{GT/AC}$ (rpm)	4.000E+04
N_{FC} (rpm)	4.000E+04
m_{20} ($kg\,s^{-1}$)	0.000E+00
m_{23} ($kg\,s^{-1}$)	0.000E+00
$m_{17}m_{21}/m_{10}m_{13}$	1.000E+00

limit. In particular, air compressor map dramatically restricts the feasible solution region, since its operating point is very close to its surge line.

In the present simulation, the partial load operation is obtained varying only air and fuel flow rates (first and second items) and combustor bypass (third items). Air bypass factor (fourth item) is automatically handled by the simulation code in order to match the constraints about the maximum cell temperature and the maximum TIT. As above-mentioned, in the present simulation the AC–GT rotor speed (fifth item) variation is not considered. In particular, the following partial load strategies are implemented in the present analysis:

(A) constant air mass flow rate, variable fuel flow rate, no combustor bypass;
(B) constant air to fuel mass flow rate ratio, no combustor bypass;

Table 6
Main results of the simulation at full-load

Parameter	Value
HE1 efficiency	9.02E−01
HE2 efficiency	9.06E−01
HE_{SOFC} efficiency	2.66E−01
Stack efficiency	5.02E−01
$Stack_{revers.}$ efficiency	7.24E−01
GT_{is} efficiency	8.51E−01
AC_{is} efficiency	8.13E−01
FC_{is} efficiency	7.41E−01
Inverter efficiency	9.70E−01
Electrical generator efficiency	9.40E−01
Plant net electrical power (kW)	1.47E+03
Plant net thermal power (kW)	4.89E+02
Plant ex_d (kW)	4.89E+02
Plant fuel (kW)	2.35E+03
Plant exergetic residual (kW)	2.99E+02
Plant net electrical efficiency	6.54E−01
Plant net thermal efficiency	2.18E−01
Plant net exergetic efficiency	6.26E−01

(C) constant air mass flow rate, variable fuel flow rate and combustor bypass.

The first criterion is obviously the simplest one since the partial load operation is achieved regulating the downstream valve of the fuel compressor. On the other hand, this strategy does not allow a satisfactory control of both the stack and the GT inlet temperatures since, reducing the fuel to air ratio, these temperature decrease lowering the system efficiency. Stack temperature and TIT can be better controlled handling also the air flow rate or bypassing some fuel mass flow rate directly to the combustor (B and C strategy). In the following, details are supplied for each partial load control strategy.

17.1. Strategy A

The first criterion is based on the reduction of the fuel flow rate, fixing the air mass flow rate allowing a significant reduction of plant net electrical power production, since it can be reduced down to 35% of its nominal value (Fig. 12a). As reported in literature [1–3], the SOFCs achieve electrical efficiencies close to their nominal value at partial load too. In spite of this, the global hybrid SOFC–GT power plant electrical efficiency significantly

Table 7
Components energy, exergy flows and efficiencies, at full-load operation

	Q (kW)	L (kW)	S_{gen} ($kW\,K^{-1}$)	ex_d (kW)	η_{ex}	δ (%)
AC	0.00E+00	5.38E+02	1.84E−01	5.48E+01	8.98E−01	1.12E+01
FC	0.00E+00	2.40E+01	1.30E−02	3.86E+00	8.39E−01	7.89E−01
GT	0.00E+00	9.04E+02	1.80E−01	5.37E+01	9.44E−01	1.10E+01
HE1	6.27E+02	0.00E+00	7.34E−02	2.18E+01	9.43E−01	4.45E+00
HE2	1.99E+01	0.00E+00	7.76E−03	2.32E+00	8.00E−01	4.74E−01
M	0.00E+00	0.00E+00	8.15E−02	2.43E+01	9.92E−01	4.96E+00
CB	0.00E+00	0.00E+00	3.50E−01	1.04E+02	9.48E−01	2.13E+01
IRSOFC	0.00E+00	1.22E+03	6.47E−01	1.93E+02	8.63E−01	3.94E+01
HE_{SOFC}	3.05E+02	0.00E+00	1.07E−01	3.19E+01	8.66E−01	6.51E+00
MGT	0.00E+00	0.00E+00	0.00E+00	0.00E+00	0.00E+00	0.00E+00

Table 8
State-points main properties at full-load operation

k-Point	Temperature (°C)	Pressure (bar)	Enthalpy (kJ kg^{-1})	Entropy (kJ kg^{-1} K^{-1})	Physical exergy (kJ kg^{-1})	Chemical exergy (kJ kmol^{-1})	Mass flow (kg s^{-1})	xH$_2$O	xCO	xH$_2$	xO$_2$	xN$_2$	xCO$_2$	xCH$_4$
1	3.66E+02	7.27E+00	9.95E+02	1.27E+00	6.33E+02	8.20E+05	4.65E−02	0.00E+00	0.00E+00	0.00E+00	0.00E+00	2.00E−02	0.00E+00	9.80E−01
2	8.24E+02	7.20E+00	1.57E+03	2.30E+00	1.03E+03	2.21E+05	2.82E−01	4.49E−01	4.51E−02	6.18E−02	0.00E+00	9.79E−03	2.10E−01	2.24E−01
3	1.02E+03	7.06E+00	1.68E+03	2.16E+00	1.15E+03	4.49E+04	4.42E−01	5.82E−01	5.85E−02	8.02E−02	0.00E+00	6.76E−03	2.73E−01	0.00E+00
4	1.02E+03	7.06E+00	1.68E+03	2.16E+00	1.15E+03	4.49E+04	2.07E−01	5.82E−01	5.85E−02	8.02E−02	0.00E+00	6.76E−03	2.73E−01	0.00E+00
5	1.02E+03	7.06E+00	1.68E+03	2.16E+00	1.15E+03	4.49E+04	2.35E−01	5.82E−01	5.85E−02	8.02E−02	0.00E+00	6.76E−03	2.73E−01	0.00E+00
6	7.51E+02	7.16E+00	8.05E+02	9.79E−01	5.58E+02	1.29E+02	1.89E+00	0.00E+00	0.00E+00	0.00E+00	2.10E−01	7.90E−01	0.00E+00	0.00E+00
7	1.02E+03	7.02E+00	1.12E+03	1.23E+00	7.93E+02	1.66E+02	1.72E+00	0.00E+00	0.00E+00	0.00E+00	1.44E−01	8.56E−01	0.00E+00	0.00E+00
8	1.15E+03	6.74E+00	1.34E+03	1.55E+00	9.50E+02	8.24E+02	1.93E+00	8.21E−02	0.00E+00	0.00E+00	1.19E−01	7.58E−01	4.10E−02	0.00E+00
9	1.02E+03	6.74E+00	1.18E+03	1.43E+00	8.27E+02	8.24E+02	1.93E+00	8.21E−02	0.00E+00	0.00E+00	1.19E−01	7.58E−01	4.10E−02	0.00E+00
10	6.40E+02	1.14E+00	7.15E+02	1.53E+00	3.31E+02	8.24E+02	1.93E+00	8.21E−02	0.00E+00	0.00E+00	1.19E−01	7.58E−01	4.10E−02	0.00E+00
11	2.68E+02	1.12E+00	2.88E+02	9.35E−01	8.09E+01	8.24E+02	4.65E−02	8.21E−02	0.00E+00	0.00E+00	1.19E−01	7.58E−01	4.10E−02	0.00E+00
12	2.50E+01	1.00E+00	2.52E+01	2.36E−01	0.00E+00	1.29E+02	1.89E+00	0.00E+00	0.00E+00	0.00E+00	2.10E−01	7.90E−01	0.00E+00	0.00E+00
13	3.00E+02	7.46E+00	3.11E+02	3.34E−01	2.56E+02	1.29E+02	1.89E+00	0.00E+00	0.00E+00	0.00E+00	2.10E−01	7.90E−01	0.00E+00	0.00E+00
14	2.50E+01	1.00E+00	5.24E+01	2.34E−01	0.00E+00	8.20E+05	4.65E−02	0.00E+00	0.00E+00	0.00E+00	0.00E+00	2.00E−02	0.00E+00	9.80E−01
15	2.29E+02	7.42E+00	5.68E+02	5.12E−01	4.33E+02	8.20E+05	4.65E−02	0.00E+00	0.00E+00	0.00E+00	0.00E+00	2.00E−02	0.00E+00	9.80E−01
16	6.40E+02	1.14E+00	7.15E+02	1.53E+00	3.31E+02	8.24E+02	4.65E−02	8.21E−02	0.00E+00	0.00E+00	1.19E−01	7.58E−01	4.10E−02	0.00E+00
17	6.40E+02	1.14E+00	7.15E+02	1.53E+00	3.31E+02	8.24E+02	1.89E+00	8.21E−02	0.00E+00	0.00E+00	1.19E−01	7.58E−01	4.10E−02	0.00E+00
18	6.07E+02	7.31E+00	6.43E+02	8.03E−01	4.49E+02	1.29E+02	1.89E+00	0.00E+00	0.00E+00	0.00E+00	2.10E−01	7.90E−01	0.00E+00	0.00E+00
19	3.52E+02	1.12E+00	3.83E+02	1.10E+00	1.27E+02	8.24E+02	1.89E+00	8.21E−02	0.00E+00	0.00E+00	1.19E−01	7.58E−01	4.10E−02	0.00E+00
20	2.50E+01	1.00E+00	–	–	–	–	0.00E+00	0.00E+00	0.00E+00	0.00E+00	0.00E+00	0.00E+00	0.00E+00	0.00E+00
21	1.02E+03	6.74E+00	1.18E+03	1.43E+00	8.27E+02	8.24E+02	1.93E+00	8.21E−02	0.00E+00	0.00E+00	1.19E−01	7.58E−01	4.10E−02	0.00E+00
22	6.07E+02	7.31E+00	6.43E+02	8.03E−01	4.49E+02	1.29E+02	1.89E+00	0.00E+00	0.00E+00	0.00E+00	2.10E−01	7.90E−01	0.00E+00	0.00E+00
23	2.50E+01	1.00E+00	–	–	–	–	0.00E+00	0.00E+00	0.00E+00	0.00E+00	0.00E+00	0.00E+00	0.00E+00	0.00E+00
24	3.66E+02	7.27E+00	9.95E+02	1.27E+00	6.33E+02	8.20E+05	4.65E−02	0.00E+00	0.00E+00	0.00E+00	0.00E+00	2.00E−02	0.00E+00	9.80E−01

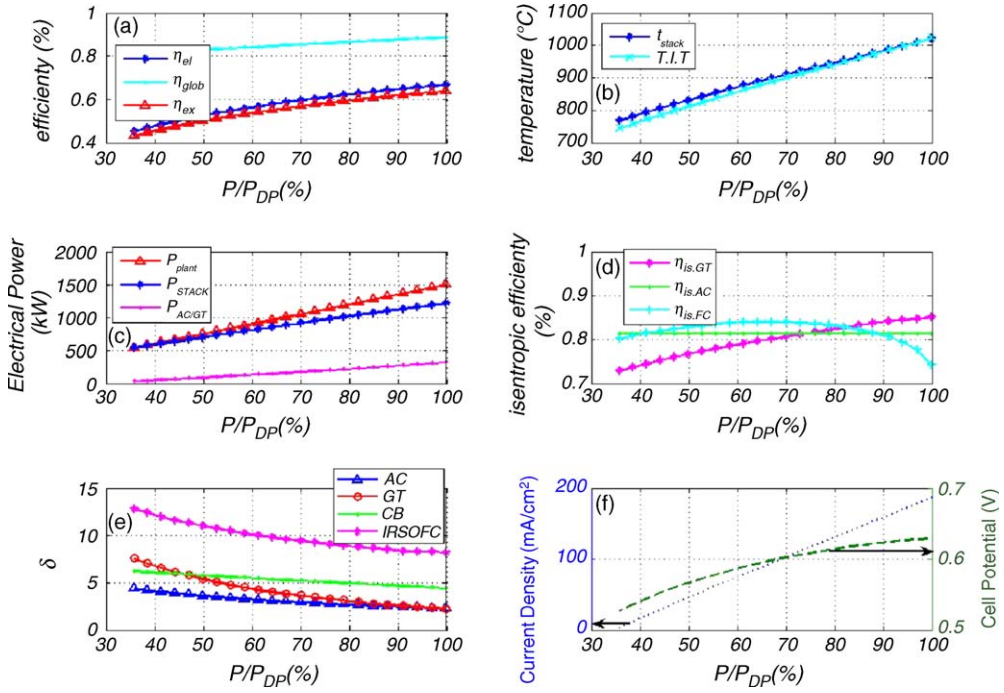

Fig. 12. Strategy A: energetic, exergetic and electrochemical results.

decreases down to 45% (Fig. 12a) mostly because of the variation of the fuel to air ratio. In fact, at partial load operation less fuel is required, consequently the fuel to air ratio decreases, determining the reduction of both TIT and stack temperature (Fig. 12b). In relation to the minimum power ratio (P/P_{DP}) of 35%, such temperatures approach 750 °C. The stack efficiency is affected by its operating temperature: even if, at partial load operation, lower values of current densities are achieved (Fig. 12f), the reduction of its operating temperature is so high that cell voltage decreases approaching 0.50 V (Fig. 12f). This phenomenon depends on the voltage trend in function of current density and temperature, previously described in Fig. 6. Here, the effect of temperature decrease is dominant with respect to the current density reduction. Furthermore, GT and FC performance significantly varies reducing the overall electricity produced by the hybrid plant. The air compressor isentropic efficiency is constant since no variation in air flow rate and in the rotor speed occurs (Fig. 12d). GT isentropic efficiency decreases with P/P_{DP} as a consequence of the reduction of its TIT (Fig. 12d). According to the typical shape of the compressor maps, the FC isentropic efficiency shows a non-monotonic variation since its design point did not achieve the highest value of its isentropic efficiency (Fig. 12d). The reduction of GT isentropic efficiency determines a remarkable growth of its exergy destruction rate and consequently of its efficiency defect (Fig. 12e). Similarly, the high values of SOFC overvoltages determine higher IRSOFC efficiency defects with respect to the full-load operation (Fig. 12e). Finally, the overall plant exergy efficiency decreases in the same way of the electrical efficiency (Fig. 12a). The higher is the reduction of output power, the higher are the irreversibilities (mainly due to the GT and the IRSOFC, Fig. 12e). In Fig. 12c, the ratio between stack and AC–GT power production is shown: at part-load operation, a decrease is detected. This behavior is due to the higher slope of the GT electrical power curve with respect to the stack one.

17.2. Strategy B

The advantage of the first partialization criterion mainly consists in the possibility to operate also in case of very low electrical loads. On the other hand, this criterion also implies a remarkable reduction of plant efficiency (Fig. 12a), mainly due to the reduction of both stack and GT inlet temperatures. For this reason, a new criterion is implemented, aiming to control such temperatures. Such strategy is obtained keeping constant the air to fuel ratio. By contrast to the first criterion, the simulation shows that the stack temperature and TIT slightly increase with the P/P_{DP} reduction (Fig. 13b). An increase of the cell voltage (Fig. 13f) is obtained as a consequence of both current density reduction (Fig. 13f) and stack temperature growth (Fig. 13b). On the other hand, the variation of the GT mass flow rate and of the TIT, determines the GT isentropic efficiency reduction (Fig. 13d). In fact, the GT operating point moves in the inefficient region of its map. This reduction is also the reason of its entropy generation increase and consequently of the higher value of its efficiency defect (Fig. 13e). The high voltages achieved by the cell (Fig. 13f), determine lower overvoltages versus the full-load operation, and consequently lower efficiency defects of the IRSOFC (Fig. 13e). The two above-mentioned effects are in contrast, but the reduction of turbomachineries isentropic efficiency is only slightly dominant so that the overall result is a small reduction of the exergetic efficiency (Fig. 13a). This part-load strategy also shows almost the same trend of the ratio between stack and GT power production reported for the strategy A (Fig. 13c). Differently from the previous criterion, this partialization procedure shows a very small operating range, since

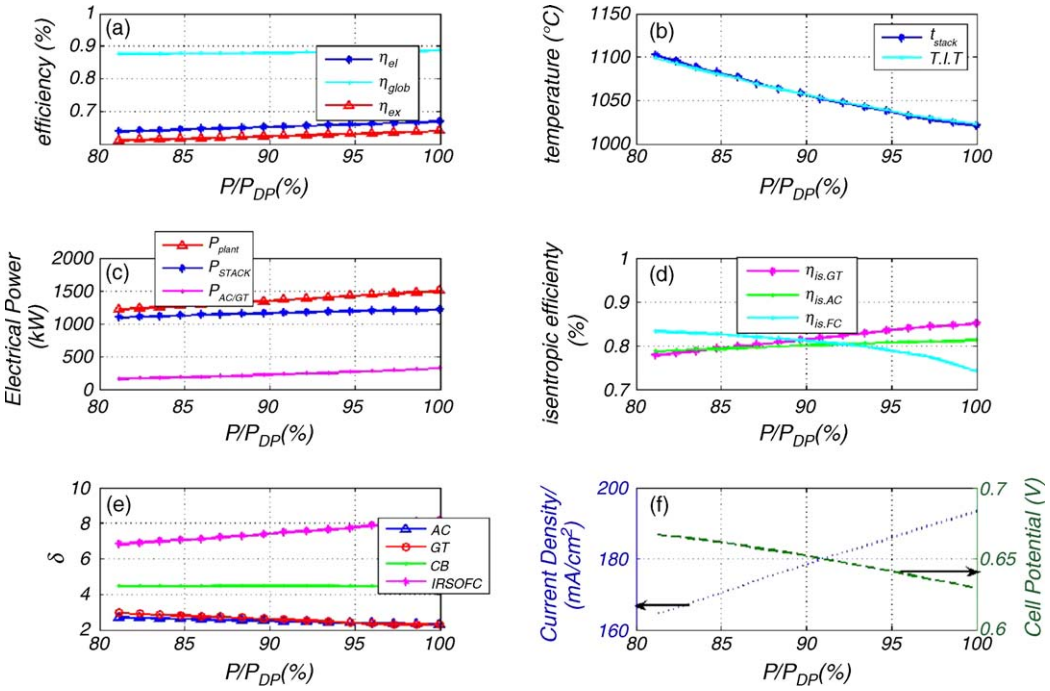

Fig. 13. Strategy B: energetic, exergetic and electrochemical results.

reducing the net electrical power more than 80% (Fig. 13a), the air compressor approaches its surge line. Obviously, a better design of such component would allow to achieve lower P/P_{DP}.

17.3. Strategy C

An other partialization procedure is introduced in order to reduce problems of GT and SOFC temperatures management, achieved by the first criterion and in order to enlarge the partialization field of the second strategy (Fig. 14a). This procedure is based on the first one, varying also the combustor bypass factor, which is linearly increased with P/P_{DP}. The aim is to increase the stack temperature and TIT with respect to the strategy B. This target is reached only in case of TIT (Fig. 14b), in fact, much more chemical energy is converted into heat. This additional heat, with respect to the no-bypass condition,

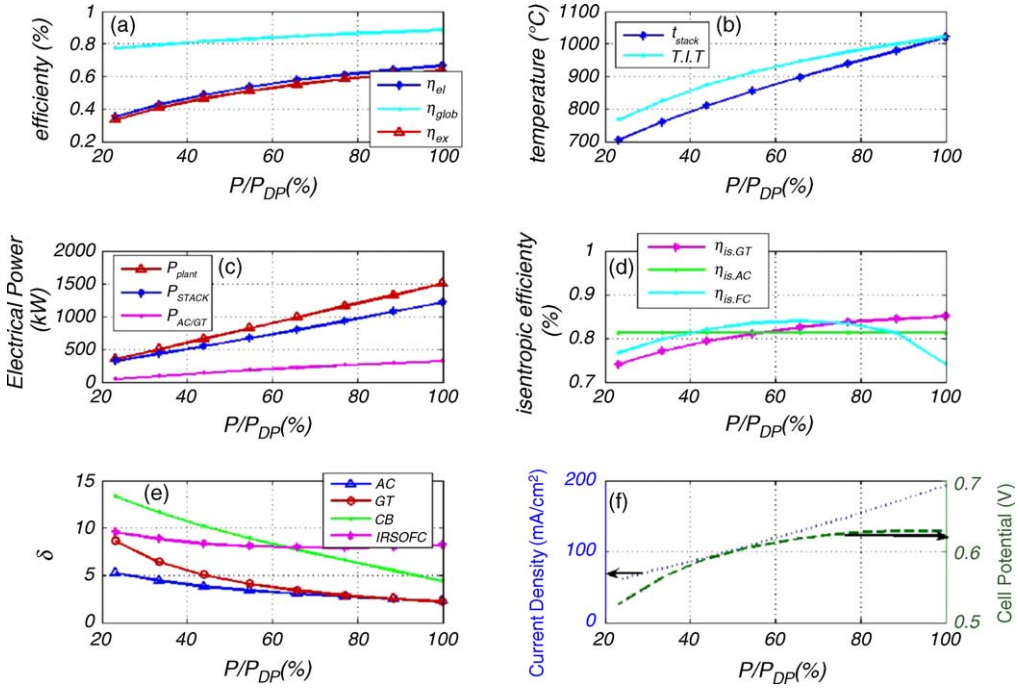

Fig. 14. Strategy C: energetic, exergetic and electrochemical results.

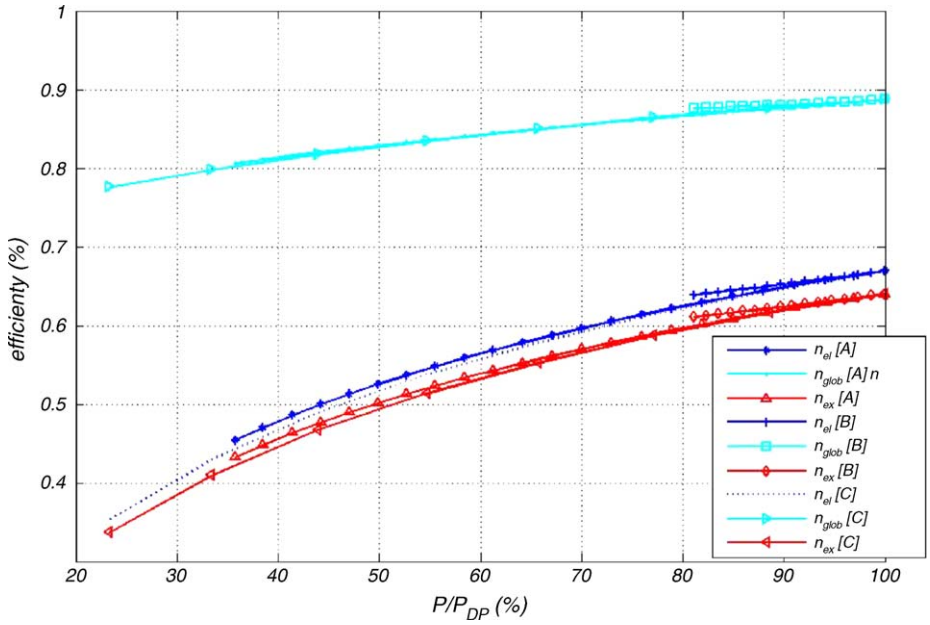

Fig. 15. Energetic and exergetic efficiencies comparison for the three partialization strategies.

is used to increase GT inlet temperature. On the other hand, less fuel is available for the electrochemical reaction, reducing also the amount of heat produced by the overall electrochemical/reforming reactions. Consequently SOFC operating temperature significantly decreases (Fig. 14b). The above-mentioned results show that the managing of the combustor by pass factor does not allow to control both TIT and stack temperature simultaneously. In order to reach this goal it is also required to reduce the air mass flow rate. Anyhow, the better control of TIT also allows to achieve higher GT isentropic efficiencies (Fig. 14d). Obviously, the compressors isentropic efficiencies, independent from TIT and stack temperature, show the same trend reported in the case of the strategy A (Fig. 14d). The same trend is also showed in case of GT and stack power production (Fig. 14c). The reduction of stack temperature causes, similarly to the first criterion, a remarkable reduction of both cell potential and current density (Fig. 14f). This reduction corresponds at a slight increase of its efficiency defect since the CB to IRSOFC conversion ratio increases (Fig. 14e). This circumstance determines a significant growth of catalytic burner efficiency defect (Fig. 14e).

18. Conclusions

In the present paper, the hybrid SOFC–GT power plant is described and simulated at both design and partial load operations. Three partial load procedures are introduced, based on the fuel and air mass flow rates variations. The simulation of partial load operation of the SOFC–GT hybrid plant shows that the best performance is achieved in case of constant fuel to air ratio. This partialization criterion allows to control both stack and GT inlet temperatures, achieving simultaneously low cell overvoltages (0.50 V cell voltage) and high GT isentropic efficiency (72%). On the other hand, this technique does not allow to reduce plant net electrical power more than 80% of its nominal value. In such range, the electrical, global end exergetic efficiencies, achieved in case of the strategy A, are slightly higher the ones resulting from the other criterions (Fig. 15). Furthermore, handling the combustor bypass ratio it is not possible to achieve better values of plant efficiencies. Their efficiency curves do not show a significant variation with respect to these ones coming from the second criterion (Fig. 15). Finally, a better behavior of the partial load operation could be achieved implementing the first criterion and optimizing the turbomachineries design. In this case an optimization procedure is required in order to find the optimum values of map scaling factor. Such values shall maximize the average net electrical efficiency, according with user load profile. Simultaneously, future works will deal also with the thermo-economic optimization of this plant, aiming at finding the set of synthesis/design parameters minimizing the overall plant cost achieved during its complete operating life.

References

[1] S.C. Singhal, K. Kendall, High temperature Solid Oxide Fuel Cells, Elsevier, 2003.
[2] J. Larminie, A. Dicks, Fuel Cell System Explained, John Wiley & Sons Ltd., 2002.
[3] AAVV, Fuel Cell Handbook, 6th ed., U.S. Department of Energy, 2002.
[4] AAVV, in: Gregors Hoogers (Ed.), Fuel Cell Technology Handbook, CRC Press, 2003.
[5] Jens Palsson, Azra Selimovic, Lars Sjunnesson, Combined solid oxide fuel cell and gas turbine systems for efficient power and heat generation, J. Power Sources 86 (2000) 442–448.
[6] S Kasagi, N. Kimijima, performance evaluation of gas turbine–fuel cell hybrid micro generation system, in: Proceedings of the ASMETURBO EXPO 2002, Amsterdam, The Netherlands, June 3–6, 2002.
[7] B.H. Bae, J.L. Sohn, S.T. Ro, Thermodynamic modeling and performance analysis of a power generation system based on the solid oxide fuel cell, in: Proceedings of the FUELCELL2003, Fuel Cell Science, Engineering and Technology, Rochester, NY, USA, April 21–23, 2003.

[8] Y. Inui, S. Yanagisawa, T. Ishida, Proposal of high performance SOFC combined power generation system with carbon dioxide recovery, Energy Conv. Manage. 44 (2003) 597–609.
[9] P. Costamagna, L. Magistri, A.F. Massardo, Design and part-load performance of a hybrid system based on a solid oxide fuel cell reactor and a micro gas turbine, J. Power Sources 96 (2001) 352–368.
[10] S. Campanari, Full load and part load performance prediction for integrated SOFC and microturbine systems, J. Power Sources 96 (2001) 352–368.
[11] S.H. Chan, H.K. Ho, Y. Tian, Modelling for part load operation of solid oxide fuel cell–gas turbine hybrid power plant, J. Power Sources 114 (2003) 213–227.
[12] S. Campanari, Power plants based on solid oxide fuel cells combined with gas turbine cycles, Ph.D. Thesis, Politecnico di Milano, Milano, 1998.
[13] F. Calise, M. Dentice d'Accadia, A. Palombo, L. Vanoli, Simulation and exergy analysis of a hybrid SOFC–gas turbine system. Part I. Description of the model, in: Proceedings of the 17th International Conference on Efficiency, Costs, Optimization, Simulation and Environmental Impact of Energy and Process Systems, Gunajuato, Mexico, Luglio 7–9, 2004.
[14] F. Calise, M. Dentice d'Accadia, A. Palombo, L. Vanoli, Simulation and exergy analysis of a hybrid SOFC–gas turbine system. Part I. Results and discussion, in: Proceedings of the 17th International Conference on Efficiency, Costs, Optimization, Simulation and Environmental Impact of Energy and Process Systems, Gunajuato, Mexico, Luglio 7–9, 2004.
[15] F. Calise, M. Dentice d'Accadia, A. Palombo, L. Vanoli, R. Vanoli, Modelling, simulation and exergy analysis of a hybrid SOFC–gas turbine system, in: Proceedings of the Third International Symposium Energy and Environment, Sorrento, 30 September–2 October, 2004.
[16] Kai W. Bedringas, Ivar S. Ertesvag, Exergy analysis of solid oxide fuel cell systems, Energy 22 (1997) 403–412.
[17] W.R. Dunbar, N. Lior, R. Gaggioli, Combining fuel cells with fuel-fired power plants for improved exergy efficiency, Energy: Int. J. 16 (10) (1991) 1259–1274.
[18] W.R. Dunbar, N. Lior, R. Gaggioli, The effect of the fuel-cell unit size on the efficiency of a fuel-cell-topped Rankine Cycle, ASME J. Energy Resour. Technol. 115 (1993) 105–107.
[19] S.H Chan, C.F. Low, O.L. Ding, Energy and exergy analysis of a simple solid-oxide fuel cell power system, J. Power Sources 103 (2002) 188–200.
[20] T.J. Kotas, The Exergy Method of Thermal Plant Analysis, Butterworths, 1985.
[21] S. Kakac, H. Liu, Heat Exchangers, Selection, Rating and Thermal Design CRC Press LLC, 1998.
[22] Kays, London, Compact Heat Exchangers, 3rd ed., 1998.